RSC Advances

ROYAL SOCIETY OF CHEMISTRY

www.rsc.org/advances

Investigation of Ce(III) promoter effects on the tri-metallic Pt,Pd,Ni/MgO catalyst in dry-reforming of methane

Faris A. J. Al-Doghachi[a,b], Umer Rashid[c], Yun Hin Taufiq Yap[a,b*]

[a]Catalysis Science and Technology Research Centre, Faculty of Science, University Putra Malaysia, 43400, UPM, Serdang, Selangor, Malaysia.

[b]Department of Chemistry, Faculty of Science, University Putra Malaysia, 43400, UPM, Serdang, Selangor, Malaysia.

[c]Institute of Advanced Technology, University Putra Malaysia, 43400, UPM, Serdang, Selangor, Malaysia.

*Corresponding author:

Prof. Dr. Yun Hun Taufiq-Yap
Catalysis Science and Technology Research Centre
Faculty of Science, University Putra Malaysia, 43400 UPM Serdang
Selangor, Malaysia.
Email: taufiq@upm.edu.my
Tel: + 60-3-89466809; Fax: + 60-3-89466758

Abstract: A mixture of cerium oxide and magnesium oxide supports with certain mole ratios of Mg^{2+}/Ce^{3+} were prepared via the co-precipitation of Mg and Ce nitrates, and followed by impregnation with 1 wt.% each of Ni, Pd, and Pt metals to form Pt,Pd,Ni/$Mg_{1-X}Ce_XO$ catalysts. Evaluation of the prepared catalysts was carried out by a DRM reaction for 200 h and characterised by means of in situ XRD, XRF, XPS, BET, H_2-TPR, TEM and TGA. It was found that the interaction of a suitable amount of MgO with Ce_2O_3 stabilised cubic phase in catalysts, which has a high basicity to adsorb CO_2 forming monoclinic $Ce_2O_2CO_3$ species in the DRM reaction. The introduction of MgO also created surface oxygen ions. The oxidisation and the removal of the deposited carbon maybe achieved by both monoclinic $Ce_2O_2CO_3$ and surface oxygen, keeping the metal Ni, Pd, and Pt catalyst at high activity and stability. The Ce_2O_3 as a promoter in the catalyst had several effects such as: stabilisation of the magnesia cubic phase; increase in its thermal stability, increase in the basicity of the support, decreasein the carbon deposition, and decrease in the reducibility of the Ni^{2+}, Pd^{2+}, and Pt^{2+} ions.

Keywords: Biogas, Dry reforming, Catalyst deactivation, Synthesis gas, H_2 production

1. Introduction

The demand for alternative energy resources has recently been on the rise due to the fast depletion of fossil fuel. Therefore, the utilisation of greenhouse gases, such as methane and carbon dioxide, as alternative energy has received much attention. It has been found that the reserves of methane are larger than crude oil reserves because methane can be produced from various sources, including shale gas, fermented wastes, and methane hydrates.[1] Methane can be transformed into synthesis gas (a mixture of H_2 and carbon CO, also known as syngas) through reforming reactions using steam, partial oxidation or carbon dioxide.

The synthesis gas is an important feedstock for fuels and/or production of chemicals in industries. Coal, petroleum, natural gas, and biomass can be converted into syngas. However, varying the H_2/CO molar ratios is required in accordance with the industrial applications of syngas. For example, the H_2/CO ratio of 2 is required for methanol synthesis[2]; whilst the ratio is controlled at 1 for dimethyl ether (DME) synthesis under the single step process.[3] In the Fisher–Tropsch process, the H_2/CO ratio is usually in the range of 1 to 2, depending on the type of fuel synthesized.[4] Consequently, the H_2/CO ratio in syngas plays an important role in fuel production. Recently, a number of studies[5] that have been carried out have focused on the indirect reduction of iron oxides using H_2 and CO as reducing agents. The indirect reduction of iron oxides involves two mechanisms: CO-based and H_2-based.[6] The two gases or syngas can be produced from the reforming of coke oven gas (COG). In this aspect, there is no limit of the H_2/CO ratio in the utilisation of syngas for the iron making processes, whereby H_2 and CO are able to individually trigger the indirect reduction in a blast furnace.

The conversion of CH_4 to the synthesis gas, which constitutes the feed for the Fischer-Tropsch syntheses, is very important from an industrial point of view. The dominant commercial method employed to produce synthesis gas is the steam reforming of methane (Eq. 1).[7]

$$CH_4 + H_2O \rightarrow CO + 3H_2 \qquad \Delta H^{\circ}_{298K} = 225.0 \text{ kJ/mol} \qquad (1)$$

However, there are several limitations to this reaction. First, the energy consumption for this reaction is higher. Next, the selectivity for CO for this reaction is poor. Finally, the reaction is unsuitable for Fischer-Tropsch syntheses because its H_2/CO ratio is high. As a result, many researchers have attempted to convert methane to syngas through the catalytic partial oxidation of methane (Eq. 2).[8]

$$CH_4 + \frac{1}{2}O_2 \rightarrow CO + 2H_2 \qquad \Delta H^{\circ}_{298K} = -22.6 \text{ kJ/mol} \qquad (2)$$

Although this conversion is only mildly exothermic, a small decrease in the selectivity of CO due to the total combustion of methane, which is a highly exothermic reaction, has resulted in a large increase in the reaction temperature. Furthermore, a high methane conversion together with a high space velocity can produce a large amount of heat in a small region of the catalyst. As it is difficult to remove this heat from the reactor, especially in equipment for large-scale purposes, the process can become difficult to control.[9]

Several researchers have proposed to reform methane catalytically with CO_2 instead of steam, to obtain high selectivity of CO and more appropriate H_2/CO ratios. They conducted the dry reforming of methane (DRM) (Eq. 3).[10]

$$CH_4 + CO_2 \rightarrow 2\,CO + 2H_2 \qquad \Delta H^{\circ}_{298K} = 247.0 \text{ kJ/mol} \qquad (3)$$

This reaction bears important environmental implications for both the greenhouse gases, methane and carbon dioxide, which can be converted into valuable feedstocks.

The main setback of the DRM reaction is coke formation, which is caused by methane decomposition (Eq. 4) and the Boudouard reaction (Eq. 5). However, it has been reported that nickel-based catalysts can be suppressed by adding promoters in the deactivation process. In fact, strong Lewis bases (e.g., MgO, CaO) that are enhanced with the chemisorb of CO_2, have resulted in the reduction of coke deposition in the reaction with C to form CO. Similar effects have been reported for lanthanide elements, such as CeO_2 and La_2O_3, that can store and release oxygen, leading to the removal of carbon in the reaction between the deposited carbon and the lattice oxygen formed in these redox oxides.[11]

$$CH_4 \rightarrow C + 2H_2 \qquad \Delta H^{\circ}_{298K} = 75.0 \text{ kJ/mol} \qquad (4)$$

$$2CO \rightarrow C + CO_2 \qquad \Delta H^{\circ}_{298K} = \text{-}172.0 \text{ kJ/mol} \qquad (5)$$

The metal, nickel, is more commonly used as the active metal in the reforming process as its relatively abundant and its cost is low. However, the only drawback is that nickel easily induces the formation of carbon leading to catalytic deactivation.[12] As a result, numerous research studies have been carried out to improve the catalytic activity and stability of nickel-based catalysts in the reforming process.[13] The deactivation of nickel-based catalysts can be suppressed by the addition of promoters, such as strong Lewis bases (e.g., MgO, CaO) enhanced with the chemisorb of CO_2, in order to reduce coke deposition in the reaction with C to form CO.[14]

It is noted that noble metals, such as Pt, Rh and Ru, are highly active towards DRM. Also, they are more resistant to the formation of carbon in comparison to other transition metals[15],

Also, promoting Ni catalysts with noble metals that include Rh, Pt, Pd or Ru adds to the activity of the catalysts that show more stability against coke deposition when compared to the other non-promoted Ni catalysts.[16] For example, bimetallic Ni–Pt that supports ZrO_2 shows higher and more stable activity for a prolonged period of time than mono-metallic Ni/ZrO_2. Hence, Ni-Pt shows potential in the industrial application for DRM.[17] Meanwhilst, the activity and stability of bimetallic Ni–Pd catalysts are much higher than the mono-metallic Ni catalyst.[18] These findings are consistent with the hypothesis that Pd helps in the prevention of the oxidation of Ni. A recent study over the promotion of Ni/MgO with Sn, Ce, Mn and Co reported higher catalytic activity and stability for Co-promoted catalysts; moreover, the coke deposition resistance was high for Sn and Co promoted catalysts. The higher catalytic activity for Co-promoted catalysts can be attributed to its high affinity for oxygen species enhancing it coke resistance properties. While Ce and Mn promoted catalysts exhibited lower catalytic performance, for Mn-promoted catalyst the agglomeration was the sole reason for its low catalytic activity and for Ce promoted catalyst lower activity was observed due to segregation of Ce as CeO_2 due to its immiscibility with MgO which lead to the larger Ni^o particles.[19]

As such, the objective of this study has been to prepare a catalyst with high activity, selectivity, stability as well as the ability to prevent carbon deposition on the catalyst during the dry reforming of the methane reaction. The Pt,Pd,Ni/$Mg_{1-X}Ce_XO$ catalysts were prepared by using the co-precipitation method that uses K_2CO_3 as a precipitant, followed by the impregnation of 1% Pt, 1% Pd, and 1% Ni using $Pt(acac)_2$, $Pd(acac)_2$, and $Ni(acac)_2$, respectively. This was followed by a study into the comparison between the catalytic stability and coke formation. In addition, the study was also investigated the effects of the concentrations of CO_2 and CH_4, concentration of the catalysts, and the temperature of the conversion of the catalytic performance

of the prepared catalysts in the dry reforming process as well as the study evaluated the stability of the catalyst. Finally, the study was examined the enhancement of the methane conversion of a stream of 1.25% oxygen gas passing through the reaction.

2. Experimental

2.1 Support and catalyst preparations

The catalysts, $Mg_{1-x}Ce_xO$ (x = 0.00, 0.03, 0.07, 0.15), were prepared using the co-precipitation method as reported previously.[20] Meanwhilst, the support MgO and promoter ceria Ce_2O_3 were prepared using a 0.1M aqueous solution of $Ce(NO_3)_3.6H_2O$ (Merck; >99.0%) and $Mg(NO_3)_2.6H_2O$ (Merck; >99.0%) as the amount in the Table 1, and 1M K_2CO_3 (Merck; >99.7%), which were used as the precipitants. The sample was washed with hot water after the filtration of the precipitant. Next, the sample was dried at 120^{o}C for 12 hours. Subsequently, it was pre-calcined in air at 500^{o}C for 5h to remove CO_2 from the precipitant. After that, the sample was pressed into disks at 600 kg/m^2, and then calcined at 1150^{o}C for 20h for enhancement of the mechanical properties and for ensuring good interaction between the support MgO and the promoter Ce_2O_3.

Table 1 shows the preparation of the catalyst. First, 1% Pt was impregnated using $Pt(C_5H_7O_2)_2$. H_2O (Acros Chemicals; >99%) which was dissolved with dichloromethane for 5h to produce $Pt(acac)_2/Mg_{1-x}Ce_x$ O. Finally, the catalysts, $Pt,Pd,Ni(acac)_2/Mg_{1-x}Ce_x$ O, were prepared by impregnating $Pt(acac)_2/Mg_{1-x}Ce_x$ O with a 1% of each Pd and Ni by using a solution of $Pd(C_5H_7O_2)_2$ (Aldrich; >99.5%) and $Ni(C_5H_7O_2)_2.H_2O$ (Acros Chemicals; >99%) in dichloromethane for 5hr, respectively. After impregnation in the air, the catalysts were dried for

12h at a temperature of 120^{o}C. The dried catalysts were crushed and sieved to particles with 80–150 or 150–250μm diameter.

2.2 Catalyst characterisation

The thermogravimetric analysis (TGA) was carried out on a Mettler Toledo TG-DTA Apparatus (Pt crucibles, Pt / Pt − Rh thermocouple) with the purge gas (nitrogen) flow rate of 30 ml min^{-1} and the heating rate of 10°C/min from 50 to 1000°C.

An X-ray diffraction analysis was performed using a Shimadzu diffractometer model XRD 6000. The diffractometer employed Cu-Kα radiation to generate diffraction patterns from powder crystalline samples at an ambient temperature. The Cu-Kα radiation was generated by Philips glass diffraction X-ray tube broad focus 2.7KW type. The crystallite size D of the samples was calculated using the Debye–Scherrer's relationship.[21] Where D was the crystalline size, λ was the incident X-ray wavelength, β was the full width at half-maximum (FWHM), and θ was the diffraction angle.

The Fourier transform infrared (FT-IR) analysis was carried out with the PerkinElmer spectrometer model 100 series (sample preparation UATR).

The total catalyst surface area was obtained using the Brunauer–Emmett–Teller (BET) method with nitrogen adsorption at −196°C. The analysis was conducted using a Thermo Fisher Scientific S.P.A (model: Surfer Analyser) nitrogen adsorption–desorption analyser.

Transmission electron microscopy (TEM) (Hitachi H7100 TEM with accelerating voltage of 10 MV) was used to determine the crystal shape and the homogeneity of the catalysts.

Field Emission Scanning Electron Microscopy (FE-SEM) was used. The sample morphology was studied with the JEOL Field Emission scanning Electron Microscope (FE-SEM) model JSM 7600F at a very high magnification by using the field emission current. The particles of the samples were glued onto an aluminium stud by using double – sided tape. Then, it was coated with gold to make sure of the better visibility of the surface and to prevent electrical charging of the sample during analysis.

The active site of the catalysts was evaluated by Temperature Programmed Reduction (H_2-TPR) using hydrogen conducted by Thermo Finnegan TPDRO 1100 apparatus Equipped with a thermal conductivity detector. In the reactor, about 0.05g of the catalyst was placed and treated under 150°C for 30min in N_2 (20 ml/min). The analysis of Hydrogen 5.51% in Argon was carried out between 50°C and 950°C under Argon flow (10°C min^{-1}, 25 ml/min^{-1}) and detected by a thermal conductivity detector.

XPS spectra were obtained using the Kratos Axis Ultra DLD system, equipped with a monochromatic Al Kα (1486.6 eV), dual x-ray sources (Al & Mg), an argon etching system for sample cleaning and depth profiling, parallel imaging XPS, AES, ISS and Vision software for controlling the system. The base pressure of the analyser chamber was 1×10^{-10}Torr. The excitation source, X-ray gun, was operated as a combination of 20 mA of emission current and 15 KV voltages. The hemispherical analyser was operated in the fixed analyser transmission (FAT) mode for both wide and narrow scanning. This value was set at 100 eV and 40 eV of the pass energy, respectively. The region of interest for the narrow scan corresponded to Mg2p, Ce3d, Pd3d, Ni3d, Pt4f and O1s photoelectron signals. The carbon charging correction refers to the binding energy of adventitious carbon at the binding energy of 285 eV. This highly sophisticated equipment is considered as a non-destructive analysis technique due to soft x-ray

production to induce photoelectron emission from the sample surface. Therefore, the equipment was able to provide information about the surface layers or thin film structures (about the top 10-100 Å of the sample).

2.3 Catalytic evaluations

The catalytic evaluation for dry reforming of methane with CO_2 (DRM) towards syngas (H_2/CO) production as the model biogas reforming was carried out using a fixed bed stainless steel micro-reactor (i.d. Ø = 6 mm, h = 34 cm). The reactor was connected to a mass flow gas controller (SIERRA instrument) and an online gas chromatography (GC) (Agilent 6890N; G 1540N) equipped with Varian capillary columns HP-PLOT/Q and HP-MOLSIV. Prior to the reaction, approximately 0.02g of the catalyst was reduced by flowing 5% H_2/Ar (30 ml min^{-1}) at 900°C and holding for 3h. The reforming reaction was performed by flowing the feed, a gas mixture consisting of CH_4/CO_2 in (2/1) and (1/1) mol, at a rate of 30 ml/min^{-1}. The reforming has been studied from 700 to 900°C at 1 atm, then holding was carried out for 10h (1 atm, GHSV = 30 ml/min^{-1}).

The reduction step was aimed to reduce the (Pd^{+2}) phase of the palladium catalyst to the Pd metal (Pd^0) phase at the active site of the catalysts. The tested catalyst was placed in the middle of a reactor vertically and held in place by plugs of quartz wool. In order to control and ensure the reaction temperature, a thermocouple was placed into the catalyst chamber. The calculations for the CH_4 and CO_2 conversions, H_2 and CO selectivity, as well as syngas (H_2/CO) ration were defined as the following equations (Eqs. 6-10).

$$CH_4 \text{ Conversion } \% = \frac{CH_{4in} - CH_{4out}}{CH_{4\,in}} * 100 \quad (6)$$

$$CO_2 \text{ Conversion } \% = \frac{CO_{2in} - CO_{2out}}{CO_{2\,in}} * 100 \quad (7)$$

$$H_2 \text{ Selectivity } \% = \frac{H_2}{2[CH_{4in} - CH_{4out}]} * 100 \quad (8)$$

$$\text{CO Selectivity } \% = \frac{CO}{[CH_{4in} - CH_{4out}] + [CO_{2in} - CO_{2out}]} * 100 \quad (9)$$

$$\frac{H_2}{CO} \text{ratio} = \frac{H_2 \text{ Selectivity } \%}{\text{CO Selectivity } \%} \quad (10)$$

3. Results and Discussion

3.1 Characterisation of the Catalysts

3.1.1 XRD patterns. Fig. 1 (a-d) illustrates the XRD patterns of the catalysts with magnesium and cerium contents. The diffraction peaks were recorded at 2θ = 37.0 (111), 42.9 (200), 62.3 (220), 74.7 (311) and 79.1° (222). This was due to the cubic form of magnesia (JCPDS file no.: 00-002-1207). Meanwhilst, the diffraction peaks recorded at 2θ = 28.6 (111), 33.1 (200), 47.5 (220), 56.4 (311), 59.1 (222), 69.4 (400), 76.7 (331) and 79.1° (420) were due to the cubic form of ceria (JCPDS file no.: 00-034-0394). The peaks were recorded at 2θ = 47.7 (116), 56.5 (115), 59.3 (304), 62.5 (104), 69.7 (224), 77.0 (317), and 79.3° (318) were attributed to the cubic form of catalyst complex (Ce-Mg-O). However, there were no diffraction peaks for the catalyst of 1% platinum, palladium, and nickel in all the patterns. This was because the amount of these elements was very small. This observation agrees with the results reported by Grange.[22] The average crystalline size was identified through the diffraction of the highest peak in the XRD patterns that used the Debye-Scherrer equation (Table 2). The findings show that the size of the crystal was inversely proportional to the increasing amount of ceria in the catalysts. This phenomenon could be linked to the effects of platinum, palladium, and nickel that remained on

the surface of the sample that inhibited the growth of magnesia crystallites. The size of the crystal was recorded at 42.2, 53.3, 48.7, and 48.0 nm for Pt,Pd,Ni/MgO, Pt,Pd,Ni/$Mg_{0.97}Ce^{3+}_{0.03}O$, Pt,Pd,Ni/$Mg_{0.93}Ce^{3+}_{0.07}O$, and Pt,Pd,Ni/$Mg_{0.85}Ce^{3+}_{0.15}O$, respectively. Clearly, the predominant crystal system for all the samples was a cubic one. This is supported by TEM and FESEM, which showed cubic shaped particles, as well. In another study, Abimanyu et al.[23] recorded the XRD pattern of MgO-Ce_2O_3 catalyst and found 38.0 nm.

For the elemental analysis of all the components in the catalyst, XRF has been used. Table 2 shows that the Ni, Pd, and Pt percentages were slightly more than 1, which was due to the incomplete precipitation of the magnesium and cerium metal precursors in the method of co-precipitation. This had a slight effect on the results.[24]

3.1.2 XPS Analysis. Fig. 2(a-e) shows the X-ray photoelectron spectroscopy (XPS) that has been used to investigate the elements O1s, Mg2p, Ce3d, Ni2p, Pd3d and Pt4f of the reduced catalyst Pt,Pd,Ni/ $Mg_{0.93}Ce_{0.07}O$. In the study of the surface of a few layers of the catalyst, measuring 3-12 nm, the spectra of the XPS revealed a few findings. In Fig. 2a, there are five distinct oxygen species for O1s. They are on the surface of the catalyst assigned to Ni-O, Ce-O, Mg-O, Pt-O and Pd-O at a binding energy of 528.5, 529.5, 532, 533 and 534 eV, respectively. In Fig. 2b, there are two distinct peaks, obtained from Mg2p, bulk Mg-O and $MgCO_3$ at a binding energy of 49 and 51 eV, respectively. Meanwhilst, Fig. 3c shows the Ce3d of Ce_2O_3. It took the range of binding energy from 925-875 eV. The highest photoelectron signal intensity in the high binding energy region is shown in Ce-O. The peaks have been recorded at 887.5eV and 882.5 eV, respectively. The $Ni2p_{3/2}$ spectrum measures 30 eV wide. It consists of four main peaks obtained from the presence of Ni-O (Fig. 2d). Pd 3d and Pt 4f give four peaks for each due to $Pt4f_{5/2}$ and $Pt4f_{7/2}$ appearring at around 75-65 eV in the catalyst (Fig. 2e-f).[25-26]

The analysis of XPS indicates that the solid solution of Ce_2O_3 - MgO shows a low and a high binding energy of 51 eV and 882.5 eV for Mg2p and Ce3d, respectively. As a result, it is imperative to transfer the electrons from Ce_2O_3 to MgO. This is to slow down the reduction of Ce_2O_3 during the preparation of the reduced catalyst. However, during the slowdown, there is an increase in the interaction between the two oxides. This leads to the segregation of Ce atoms as small particles on the surface of the catalyst, resulting in a high dispersion of Ce, which is responsible for the high level of activity of the catalyst. Furthermore, the segregated Ce particles, which have been extracted from the substrate, interact strongly with the Ce remaining on the substrate, resulting in the attenuation of their sintering. In this case, there is no formation of coke due to the high dispersion of Ce on the surface of the catalyst. Also, the Ce clusters are not big enough for the formation of coke. The TEM has indicated that a highly effective Ce_2O_3–MgO solid solution contains crystallite sizes of about 80 nm.[18]

3.1.3 H_2-TPR. The TPR experiments were conducted on the following catalysts: Pt,Pd,Ni/MgO, Pt,Pd,Ni/$Mg_{0.97}Ce^{3+}_{0.03}O$, Pt,Pd,Ni/$Mg_{0.93}Ce^{3+}_{0.07}O$, and Pt,Pd,Ni/$Mg_{0.85}Ce^{3+}_{0.15}O$ to investigate their reduction behaviour. Fig. 3(a-d) and Table 3 show the TPR profiles of these catalysts. Fig. 4a shows three well-defined reduction peaks in the TPR profile of Pt,Pd,Ni/MgO. The first reduction peak has been recorded at 130°C. This is attributed to the reduction of the PtO species in the production of Pt^0, as compared to the previous study of Mahoney et al.[27] in which it was detected at 114°C. The second reduction peak is centered at 184^{o}C. This is due to the reduction of PdO to Pd^0. Finally, the third peak was in the region of 511^{o}C. This is associated with a reduction in the NiO species that led to a strong interaction with the supporting material to produce Ni; whereas, Bao et al.[28] found the reduction temperature of NiO in the Ni/CeMgAl catalyst at 516°C.

Fig. 3(b-d) and Table 3 illustrate the TPR profile for the catalysts including the promoter Ce_2O_3. The TPR profiles for Pt,Pd,Ni/$Mg_{0.97}Ce^{3+}_{0.03}O$, Pt,Pd,Ni/$Mg_{0.93}Ce^{3+}_{0.07}O$, and Pt,Pd,Ni/$Mg_{0.85}Ce^{3+}_{0.15}O$ catalysts are quite different from the catalyst Pt,Pd,Ni/MgO. The findings show five peaks. The first three peaks of the catalyst Pt,Pd,Ni/$Mg_{0.97}Ce^{3+}_{0.03}O$ were recorded at 129^{o}C, 169^{o}C, and 481^{o}C; whilst the peaks of the catalyst Pt,Pd,Ni/$Mg_{0.93}Ce^{3+}_{0.07}O$ were recorded at 132^{o}C, 198^{o}C, and 495^{o}C. Meanwhilst, the peaks of the catalyst Pt,Pd,Ni/$Mg_{0.85}Ce_{0.15}O$ were recorded at 135^{o}C, 160^{o}C, and 490^{o}C. This was due to the reduction of PtO, PdO, and NiO on the surface of the catalysts to obtain the elements Pt^0, Pd^0, and Ni^0, respectively. The fourth peak of the catalysts Pt,Pd,Ni/$Mg_{0.97}Ce^{3+}_{0.03}O$, Pt,Pd,Ni/$Mg_{0.93}Ce^{3+}_{0.07}O$, and Pt,Pd,Ni/$Mg_{0.85}Ce^{3+}_{0.15}O$ was found where the temperatures were recorded at 502^{o}C, 508^{o}C, and 510^{o}C, respectively. The findings correspond to the reduction of Ce_2O_3 on the surface. In fact, there was a significant lowering of the surface of Ce_2O_3 when there was a reduction in the temperature of the catalysts. There are several possible explanations for this phenomenon. Firstly, it could be due to the improved dispersion of Ce_2O_3 particles during the incorporation of MgO into Ce_2O_3 and the retardation of sintering.[29] Secondly, it could be due to the strong interaction between Ce_2O_3 and Pt, Pd, and Ni metals; these occur during the overlapping of the PtO, PdO and NiO and Ce_2O_3 in the reduction of peaks. The fifth peak was recorded at temperatures of 711^{o}C, 727^{o}C, and 735°C. This is attributed to the reduction of bulk Ce_2O_3 that led to strong interactions between the species of the promoter, Ce_2O_3, and the support, MgO. It has been revealed that the catalysts show more reducibility with an increase in the loading of the promoter. This finding is in agreement with the results of previous research studies, as compared with the previous study of the cerium reduction results of Rotaru et al.[29], where the reduction of cerium took place at 490^{o}C and 790^{o}C. There is a good dispersion of promoters to the support,

and it induces a high level of interaction between the support with doping Pt, Pd, and Ni species. Indeed, the significant peak of the TPR profile recorded at temperatures between 684°C – 737°C proves that Ce_2O_3 alone can reduce the range in temperatures.[30] It is also obvious that the addition of the promoter, Ce_2O_3, is effective in the reducibility of catalysts with MgO support. This could be attributed to the acidic-basic properties of the support. It has been found that $Mg_{1-x}Ce^{3+}{}_xO$ with a higher basicity than MgO interacts more with the Ce_2O_3 promoter. Thus, the reductions in PtO, PdO, and NiO are more obvious. This is due to the redox property of $Mg_{1-x}Ce^{3+}{}_xO$.[31]

The total amount of H_2-consumption in the reduction of Pt,Pd,Ni/MgO, Pt,Pd,Ni/$Mg_{0.97}Ce^{3+}{}_{0.03}O$, Pt,Pd,Ni/$Mg_{0.93}Ce^{3+}{}_{0.07}O$, and Pt,Pd,Ni/$Mg_{0.85}Ce^{3+}{}_{0.15}O$ was calculated from the total area of the peaks. The calculations for the catalysts were 488.6, 429.1, 941.9, and 737.7 μmol/g catalyst, respectively. Based on the TPR-H_2 results, the catalyst Pt,Pd,Ni/$Mg_{0.93}Ce^{3+}{}_{0.07}O$ shows that it is the most active site amongst the other catalysts. In other words, it is the best catalyst for dry reforming of methane.

3.1.4. BET. Table 4 lists the surface area of BET, pore volume and pore radius of the support MgO for the different catalysts: Pt, Pd, Ni/$Mg_{1-x}Ce_xO$ (where x= 0.00, 0.03, 0.07, and 0.15). The surface area of BET for the catalysts Pt, Pd, Ni/MgO with a cubic structure supported with TEM was 12.4 m^2/g whilst the surface area of BET for the support MgO was 11.1 m^2/g. The higher reading for the former was due to the effects of Pt, Pd, and Ni loading on the specific surface area of the support MgO. In this case, the BET surface areas of the catalysts Pt, Pd, Ni/MgO was considerably lower than the BET surface areas of the conventional catalysts: Pt,Pd,Ni/$Mg_{0.97}Ce^{3+}{}_{0.03}O$, Pt,Pd,Ni/$Mg_{0.93}Ce^{3+}{}_{0.07}O$ and Pt,Pd,Ni/$Mg_{0.85}Ce^{3+}{}_{0.15}O$ which were recorded at 12.7, 19.8 and 12.9 m^2/g, respectively. This is because the magnesia pores were

partially covered by the layer of Pt, Pd, and Ni particles. However, the BET surface area of the MgO, that was promoted by Ce_2O_3 was almost similar to the one of the conventional catalysts Pt, Pd, and Ni with binary support.[32] In addition, the characteristics of the supported Pt, Pd, and Ni catalysts with a cubic structure included extremely low metal dispersion and small surface areas of the Pt, Pd, and a few Ni particles. This might be due to the strong interaction between the layers of Pt, Pd, and Ni and the support of MgO with the promoter Ce_2O_3. The pore volume of the catalyst, Pt,Pd,Ni/$Mg_{0.85}Ce^{3+}_{0.15}O$, was recorded at 0.22 cm^3/g. This value was slightly bigger than the value of the other catalysts which was recorded at 0.21 cm^3/g. This is in contrast to the study of Bao et al. (2015) where the pore volume of the NiCeMgAl catalyst was found to be 0.51 cm^3/g.[28]

Table 4 shows the pore radius of the different catalysts. The pore size of the support MgO was recorded at 9.9 Å; whereas, the pore size of the catalyst Pt,Pd,Ni/MgO was recorded at 9.7 Å. The pore radius of the remaining catalysts was inversely proportionate to the increase in the support of the promoter, Ce_2O_3; whereby, the pore radii of the catalysts: Pt,Pd,Ni/$Mg_{0.97}Ce^{3+}_{0.03}O$, Pt,Pd,Ni/$Mg_{0.93}Ce^{3+}_{0.07}O$ and Pt,Pd,Ni/$Mg_{0.85}Ce^{3+}_{0.15}O$ were recorded at 13.2 Å, 12.5 Å, and 12.4 Å, respectively.[33] This shows that the catalyst Pt,Pd,Ni/$Mg_{0.93}Ce_{0.07}O$ with a high surface area was able to perform better in the dry reforming of the methane reaction as compared to the other catalysts.

3.1.5. TEM. Fig. 4(a-d) shows the TEM images of the catalysts Pt,Pd,Ni/MgO, Pt,Pd,Ni/$Mg_{0.97}Ce^{3+}_{0.03}O$, Pt,Pd,Ni/$Mg_{0.93}Ce^{3+}_{0.07}O$, and Pt,Pd,Ni/$Mg_{0.85}Ce^{3+}_{0.15}O$ with cubic structures. The catalysts were calcined at 1150°C with a uniform particle distribution in the absence of free Ce_2O_3. Fig. 4(b-d) can be confirm the formation of the MgO-Ce_2O_3 solid solutions[34] with cubic oxide particles on the Pt, Pd, and Ni layers of the supported metal. The

catalyst Pt,Pd,Ni/$Mg_{0.97}Ce^{3+}_{0.03}O$ (Fig. 4b) was well dispersed with 1% of the Pt, Pd and Ni metal particles, each for the support magnesia-ceria of sizes ranging from 45 to 85 nm.[35] In addition, the TEM analysis of the catalyst, Pt,Pd,Ni/$Mg_{0.85}Ce^{3+}_{0.15}O$, indicated that an agglomeration of the nanoparticles at a specific distance between the metal crystallites had induced growth. Generally, metallic platinum, palladium and nickel, are known to catalyse this type of growth.[36] Although the size distribution obtained from the images of TEM were more realistic and accurate. The TEM results (Fig. 4a- 4e) are well in relation with XRD data which showed that the complex Mg-Ce-O were also cubic in nature like MgO and Ce_2O_3.

3.1.6. Thermal analysis study. Fig. 5(a-d) shows the analysis of the TGA for the reduced catalysts, Pt,Pd,Ni/MgO, Pt,Pd,Ni/$Mg_{0.97}Ce^{3+}_{0.03}O$, Pt,Pd,Ni/$Mg_{0.93}Ce^{3+}_{0.07}O$, and Pt,Pd,Ni /$Mg_{0.85}Ce^{3+}_{0.15}O$. The findings indicate a weight loss; but, at only one stage of the thermal process. The weight loss was recorded at about 2% at temperatures ranging from 100°C to 120°C. This could be attributed to the removal of moisture from the catalysts Pt,Pd,Ni /$Mg_{1-x}Ce_xO$ (Fig. 5a-d). Meanwhilst, the weight loss was recorded at 1.5%, 2.2%, 1.8%, and 1.6% for the catalysts: Pt,Pd,Ni /MgO, Pt,Pd,Ni /$Mg_{0.97}Ce^{3+}_{0.03}O$, Pt,Pd,Ni /$Mg_{0.93}Ce^{3+}_{0.07}O$, and Pt,Pd,Ni /$Mg_{0.85}Ce^{3+}_{0.15}O$, respectively. On the other hand, the Pt,Pd,Ni /$Mg_{0.85}Ce^{3+}_{0.15}O$ and Pt,Pd,Ni/$Mg_{0.93}Ce^{3+}_{0.07}O$, catalysts (Fig. 5c-d), showed an additional second stage. Here, the weight loss was recorded at 2% and 3%, respectively, which may be attributed to the loss of oxygen atoms from the catalysts. The graph shows that initially, the entire weight of the compound increased slightly. This was due to the adsorbing of the compound to the N_2 gas in the machine. All the compounds became thermally stable at a temperature of 500°C. This was because of the high melting point of magnesia and ceria at 2852°C and 2177°C, respectively. Fig.

5(a-d) reveals that the components of the catalyst show good interaction components. This is in agreement with the results of Mojovic et al.[37]

3.2. Catalytic performance in biogas reforming

3.2.1. Effect of the reactant concentration on conversion. The reaction activity of the dry reforming of methane was indicated by the conversion of CH_4 and CO_2, and the selectivity was expressed in terms of the H_2/CO ratio. When the temperature was set above 900°C, the findings of the blank tests (reaction without catalyst) revealed the presence of H_2 and CO in the outlet gas. This may be due to the decomposition reaction of methane (Eq. 5). When $Mg_{1-x}Ce_xO$ was used without Pt, Pd, and Ni metals, the conversion of CH_4 and CO_2 was very low, recording 38% and 48%, respectively; whilst, the H_2/CO ratio was recorded at 0.2 %. These results indicate that the reaction on the pores of the support promoter was weak. Likewise, the BET results also showed that there were pores in the catalyst. On the other hand, when the catalysts Pt,Pd,Ni/$Mg_{1-x}Ce^{3+}{}_xO$ were used, the conversion of CH_4 and CO_2 and the ratio of H_2/CO showed an increase (Fig. 6). This means that the Pt, Pd, and Ni metals doped on the support play a crucial role in the catalytic reaction. The catalyst Pt,Pd,Ni/$Mg_{0.93}Ce^{3+}{}_{0.07}O$ recorded a CH_4 and CO_2 conversion in 83 % and 97 % for CH_4: CO_2 (2:1), respectively, and the H_2: CO ratio of 1.15. However, the conversion of the gases, CH_4:CO_2 at the ratio of (1:1) was 84 %, 99 % and 1.2, respectively. This indicates that the ratio of 1:1 provides the best resistance to the deactivation of the catalyst. The reason for this is the carbon formation and high selectivity of H_2 and CO (Fig. 6). The other catalysts have also been shown to be similar in this aspect.[38]

3.2.2. Effect of the catalyst concentration on conversion. Fig. 7 and Table 5 show the effects of the concentration of the catalyst during the conversion process. The conversion of CH_4, CO_2

and the ratio of H_2/CO were in an ascending order as in: Pt,Pd,Ni/MgO<Pt,Pd,Ni/$Mg_{0.97}Ce^{3+}_{0.03}O$<Pt,Pd,Ni /$Mg_{0.85}Ce^{3+}_{0.15}O$ < Pt,Pd,Ni / $Mg_{0.93}Ce^{3+}_{0.07}O$.

The Pt and Pd were combined with nickel on the support, MgO-Ce_2O_3. The experiments were conducted under the following conditions: a temperature of 900°C and 1 atm with a feed ratio (CH_4:CO_2) of 1:1 (Fig. 7 & Table 5). As for the conversion of methane, the highest conversion recorded was found in the catalyst Pt,Pd,Ni/$Mg_{0.93}Ce^{3+}_{0.07}O$ (84%); whilst, the lowest conversion was observed in the catalyst Pt,Pd,Ni/MgO (75%). Another finding is that most of the catalysts tested showed a slight deactivation after 200h. Overall, the conversion of CO_2 was more stable than for methane; and, for the conversion of CH_4, the highest conversion was found in the catalyst Pt,Pd,Ni/$Mg_{0.93}Ce^{3+}_{0.07}O$ (99%); whilst, the lowest conversion was observed in the catalyst Pt,Pd,Ni/MgO (86%). From the readings, it can be concluded that the best catalyst is Pt,Pd,Ni / $Mg_{0.93}Ce^{3+}_{0.07}O$.

The product ratio of H_2/CO over all the tri-metallic magnesia-ceria catalysts (Fig. 7 & Table 5) was recorded at above 1. This indicated that the process of CO_2 conversion of the Ni metal was less favourable than that of the tri-metallic catalysts as compared to the other studies.[28] Also, the side reactions showed improvement. This is evident from the observed difference between the conversions and the product yields. Table 5 shows that with an increase in the concentration of ceria, there were increases in the conversion rate of CH_4 and CO_2 as well as the ratio of H_2/CO. The best result observed by the catalyst Pt,Pd,Ni / $Mg_{0.93}Ce^{3+}_{0.07}O$ was found at the most active site of H_2-TPR and from the large surface area indicated from the BET result. This phenomenon reveals that the incorporation of Ce_2O_3 into the MgO catalysts can significantly depress the Reverse Water Gas Shift (RWGS) reaction (Eq.11).

$$CO_2 + H_2 \rightarrow CO + H_2O \qquad \Delta H^{\circ}_{298K} = 41.0 \text{ kJ/mol} \qquad (11)$$

The results also indicate that the rate of the CO formation in the dry reforming of methane was dependent on the strong interaction between the promoter, Ce_2O_3, and the support, MgO solid solution, based on the following findings: the ratio of 0.07:0.93 mole in the catalyst, the largest surface area of 19.8 m^2/g (Table 4), and the most active site of 941.9 μmol/g from the total amount of H_2-consumption in the H_2-TPR study (Table 3). Hence, the formation of a solid solution was crucial in the generation of the active sites for the CO_2 reforming of methane.

This took place because the entire promoter, Ce_2O_3, was present as a solid solution, which stabilised both oxides. Only the surface layer of Ce_2O_3 of the solid solution of the catalyst Ce_2O_3–MgO was reduced during the reduction of hydrogen at 700°C. Furthermore, the Ce sites generated remained in close contact with the solid solution, which became a hindrance to the Ce sintering.[39] Furthermore, the sites that were responsible for the catalytic process can be found in the Pt, Pd, and Ni particles. This is because the Pt, Pd, and Ni particles have a strong interaction with MgO-Ce_2O_3. When there was an increase in the concentration of Pt, Pd, and Ni in the support, there were no significant changes in the CH_4 and CO_2 conversion and selectivity. This can be attributed to the formation of nanoparticles as a result of the XRD results (See Debye Sherrer's equation) and TEM results (See Table 2). It is known that the size distribution obtained from TEM images tends to be more realistic and accurate. However, the images have presented some limitations. On the one hand, X-ray diffraction provided a very simple possible estimation of the crystal size from the broadening of the XRD reflections through the use of Scherrer's formula. On the other hand, nanoparticulation of the particles is a preferred choice. The use of the selected nanoparticles as catalysts for this research study not only maximised the surface area

but secured more reaction. Also, it ensured a good dispersion of the Pt, Pd, and Ni metals on the surface of the catalysts, as well as strong Lewis basicity with metal oxide support. The increase of the support in Lewis basicity enhanced the ability of the catalyst to chemisorb CO_2 in the dry reforming of methane. Also, the adsorbed CO_2 reacted with C to form CO (Eq. 12), resulting in the reduction in coke formation.

$$CO_2 + C \rightarrow 2CO \qquad \Delta H^{\circ}_{298K} = +172\ kJ/mol \qquad (12)$$

The formation of the Ce_2O_3–MgO solid solution served as a unique approach in the prevention of carbon deposition. MgO is a strong Lewis base, with a high adsorption of CO_2 in reducing or preventing carbon deposition. Furthermore, the XPS results revealed that the reduction of Ce_2O_3 in the solid solution of Ce_2O_3–MgO was much more difficult, often leading to the formation of smaller particles of cerium on the surface than that of pure Ce_2O_3.[40,41] The combination of the surface basicity and the particle size of the small metals made-up the ability of the catalyst, MgO-based solid solution, in the prevention of carbon deposition. Although the size distribution obtained from the TEM images tended to be more realistic and accurate, there were some setbacks in the images.

Furthermore, the conversion of CH_4 and CO_2 was very high due to the particle size involved in the reactive activity. The doping metals, Pt, Pd, and Ni, were prepared based on the Debye Sherrer equation, and supported by the TEM analysis. The metal size had to be as minute as nanoparticles. Thus, it is evident that particle size plays a significant role in the activity of the reaction. An increase in the conversion of the reactants and selectivity (yield) was mainly due to the reduction of the particles in nano-ranged sizes leading to an increase in active sites which

was recorded at 941.9 μmol/g, and in the surface area which was recorded at 19.8 m^2/g (refer to Tables 3 & 4).

3.2.3. Effect of temperature on conversion. Fig. 8 shows the result of the activity and selectivity of catalyst Pd,Pd,Ni/ $Mg_{0.93}Ce^{3+}_{0.07}O$ at temperatures ranging from 700°C to 900°C. Generally, the conversion of CH_4:CO_2 (1:1) increased as the temperature was raised from 700°C to 900°C. This was because the dry reforming of the methane reaction showed a strong endothermic reaction (Eq. 3) and a higher temperature increased the conversion rate. This has been observed in previous studies.[42] When the temperature was increased from 700°C to 900°C, the CH_4 conversion of Pd,Pd,Ni/ $Mg_{0.93}Ce^{3+}_{0.07}O$ showed an increase from 48% to 54%; whilst the CO_2 conversion showed an increase from 18% to 74%. At temperatures above 900°C, there was no significant increase in the conversions of CH_4 and CO_2. Fig. 9 shows the H_2/CO ratio of the catalyst at various temperatures; when the temperature was <900°C, the H_2/CO ratio of the samples was recorded as <1. This was because the reverse water gas shift reaction (RWGS), (Eq. 11) consumed additional H_2 and produced CO; thereby lowering the H_2/CO ratio. At a temperature of 900°C, the H_2/CO ratio of Pd,Pd,Ni/ $Mg_{0.93}Ce^{3+}_{0.07}O$ was recorded at 1.16, indicating a smaller contribution from the RWGS reaction (Eq. 11).[15]

3.2.4. Stability tests. Fig. 9 shows the reading of the temperature tests. The findings revealed that when the temperature was at 900°C, the conversion for both CH_4 and CO_2 was high. Generally, in this mechanism, a molecule of methane reacts on the surface of Ni to produce desorbed hydrogen and hydrocarbon species CH_x (x=0-4); If x=0, the carbon deposition on the Ni metal surface[43] is indicated, as in the mechanism shown below:

$$CH_4 + 2Ni_{(as)} \longrightarrow CH_3Ni_{(as)} + HNi_{(as)}$$

$$CH_3Ni_{(as)} + Ni_{(as)} \longrightarrow CH_2Ni_{(as)} + HNi_{(as)}$$

$$CH_2Ni_{(as)} + Ni_{(as)} \longrightarrow CHNi_{(as)} + HNi_{(as)}$$

$$CHNi_{(as)} + Ni_{(as)} \longrightarrow CNi_{(as)} + HNi_{(as)}$$

$$2HNi_{(as)} \longrightarrow H_{2(g)} + 2Ni_{(as)}$$

Nakamura et al.[44] stated the effects of a promoter in the catalyst on the dry reforming of methane. One of them was by increasing the dispersion of Pt, Pt and Ni, carbon dioxide was activated on the support - promoter in proximity to the metal particle to form a carbonate species. Following that, the CH_x species reduced the carbonate to form carbon monoxide (CO).

$$CO_{2(g)} \longrightarrow CO_{2(support)}$$

$$CO_{2(support)} + O^{2-}{}_{(support)} \longrightarrow CO_3{}^{-2}{}_{(support)}$$

$$2H_{(metal)} \longrightarrow 2H_{(support)}$$

$$CO_3{}^{-2}{}_{(support)} + 2H_{(support)} \longrightarrow HCO_2{}^{-1}{}_{(support)} + OH^{1-}{}_{(support)}$$

$$CO_{(support)} \longrightarrow CO_{(g)}$$

The role of the promoter Ce_2O_3 in the catalyst was to provide a highly stable platform and a strong resistance to coking that takes place during the conversion of CO_2 and CH_4 as well as a H_2/CO ratio for over 200h of reaction. The formation of carbon on the catalyst during the dry reforming of the methane reaction was removed by Ce_2O_3. Also, the CO_2 adsorption was enhanced in the presence of Ce_2O_3 as Ce_2O_3 can increase the basicity. The next stage after adsorption, was the formation of the carbonate species. It occurred mostly on Ce_2O_3; whereby, it

dissociated to CO_2 and then to CO and O. Then O atom is transferred to Ce promoter and finally combine with the C which was deposited on the metal catalyst to produce CO.[45] It was evident that there was remarkable decrese of carbon deposition on the catalyst. When the concentration of the Ce_2O_3 was low, the CO_2 conversion showed an increase in the formation of strong ionic oxides, $Ce_2O_2CO_3$, which resulted in the attraction of CO_2 to the surface of the catalyst thereby increasing CH_4 conversion. When the concentration of Ce_2O_3 was high, the conversion of both CH_4 and CO_2 showed a decrease. This probably took place because of an increase in the electron density of Pt, Pd, and Ni.[46] The $Ce_2O_2CO_3$ species participated directly in DRM by decomposing to produce CO and to provide an oxygen species to react with the carbon deposits on the interface of Pt, Pd, and Ni -$Ce_2O_2CO_3$; thus, restoring the activity of the Pt, Pd, and Ni sites. Similarly, the Ce_2O_3 supported catalysts can facilitate the dissociation of adsorbed CO_2. In addition to its promotional effect on CO_2, the dissociative adsorption of ceria can also improve the dispersion and stabilisation of small metal particles. In fact, ceria is one of the oxides known to exert strong interactions on the supported metallic phase, resulting in significant alterations of the surface properties of both the oxide and metal.[47]

$$CO_{2(g)} \longrightarrow CO_{(support)} + O_{(promoter)}$$

$$C_{(metal)} + O_{(promoter)} \longrightarrow CO_{2(g)}$$

The activity and stability of the tri-metallic catalyst Ni–Pd-Pt was much higher than that of the mono-metallic catalyst Ni, or bi-metallic catalysts Pd-Ni and Pt-Ni. This is consistent with the hypothesis that Pt and Pd help prevent oxidation of Ni due to an increase in its electron density.[48] The formation of a Pt–Ni or Pd-Ni bi-metallic cluster increases the reducibility of Ni, resulting in higher and more stable activity for experiments of over 200h.[49]

3.2.5. Post-reaction characterization. The TEM images and TGA analysis detected the presence of a coke deposit with an oxygen stream of spent catalyst. Fig. 4f shows the TEM images. The images show that the original structure of the catalyst was maintained even after 200h of stream testing. Furthermore, the spent catalyst kept its two-dimensional cubic texture. However, there was an obvious increase in pore size from 12.2 ^{o}A to 15.6 ^{o}A, in the spent catalyst. The BET analysis also showed that the surface area of the spent catalyst was slightly increased from 19.8 to 20.2 m^2/g. The phenomenon of a slight metal sintering was observed in the spent catalyst. Whilst the two-dimensional cubic channel of spent catalyst limited the sintering of the active metals inside the pore, the active metals supported on the outside surface experienced significant sintering. Since no filamentous carbon was found in the spent catalyst, it can be concluded that the coke deposition was negligible.

Fig. 10 shows the TGA results with an oxygen stream of post-reaction tri-metallic catalyst Pt,Pd,Ni/$Mg_{0.93}Ce^{3+}_{0.07}O$ together with the calculation of weight change at each temperature range illustrated at the thermo-gram. There are altogether three different regions of temperature. The first region is the low temperature range. Here, the spent catalyst experienced an increase in weight. The second region is the mid temperature range. The spent catalyst experienced a decrease in weight in this region. The third region is the high temperature range. The spent catalyst found here experienced an increase in weight. The oxidation of the Ni particles at temperatures above 100°C caused the increase in weight. Zhu et al.[50] reported the increase in weight of the spent catalyst as less than 1%. The compound was found to be stable in the range of the temperatures (150-500)^{o}C; whilst the loss of weight at a temperature of 650°C was due to the oxidation of deposited carbon. It was found that the carbon deposited on the spent catalyst was layered carbon, with further support in the absence of filamentous carbon from the TEM

results of the spent catalysts. The amount of coke deposited on the spent catalyst was calculated to be 2.4 wt.%. Finally, all elements on the surface were 26ynthesi by oxygen after the removal of carbon on the surface as CO_2. In conclusion, the results showed that at 900^{o}C, there was little deposition of coke on the surface of the catalyst, and the formation of the coke was related to the dispersion of metal in the catalysts. The size of the smaller crystal metal catalysts makes it less prone to deactivation.

3.2.6. Improvement in the stability and selectivity of the catalyst. The dry reforming of the methane reaction can be enhanced by conducting experiments in concentrations of low oxygen flow (1.25%). Fig. 11 shows enhancement in the conversion of CH_4, from 84% to 96%, due to the addition of an oxidant (O_2) to partially or completely 26ynthes the methane as well as the use of exothermicity of the reaction to supply the necessary heat directly to the DRM reactant mixture.[46] However, the CO_2 conversion and the H_2/CO ratio are not affected. This may be due to the reaction of oxygen with CH_4 to produce CO and H_2O (Eq. 13). Finally, the steam reacts with the deposited carbon to produce syngas (Eq. 14). Furthermore, O_2 can reduce coke deposition on the catalyst (Eq. 15). Therefore, this process has reduced the deposition of carbon; consequently improving the life time of the catalyst.

$$CH_4 + 1.5O_2 \rightarrow CO + 2H_2O_{(v)} \quad (13)$$

$$C(s) + H_2O \rightarrow CO + H_2 \quad (14)$$

$$C(s) + O_2 \rightarrow CO_2 \quad (15)$$

4. Conclusions

It is inevitable that biogas is an attractive carbon source for the production of clean fuels and chemicals because it is renewable, easily available, and inexpensive. In addition, its processing,

storage and usage employs technologies and infrastructure that are developed for natural gas. Meanwhilst, the dry reforming of biogas is a promising technology in the production of syngas. In terms of 27ynthesized carbon, this approach is highly beneficial, as both major constituents of biogas (CH_4 and CO_2) are incorporated into the final hydrocarbon product. The main catalysts of Ni, Pd, Pt supported on MgO and MgO–Ce_2O_3 with cubic structures that were 27ynthesized using the co-precipitation method with K_2CO_3 as the precipitant has yielded good CO_2 and CH_4 conversion rates of 99% and 80%, respectively, for DRM at 900°C. They also showed good thermal stability for the first 200h. The supported catalysts, Pt,Pd,Ni /MgO and Pt,Pd,Ni/MgO–Ce_2O_3, with cubic structures showed good activity and thermal stability for the types of dry reforming of methane and the partial oxidation of methane reactions. These two steps occur alternately during the reforming process of the methane with the catalysts: Pt,Pd,Ni/MgO and Pt,Pd,Ni/MgO–Ce_2O_3. This occurrence ensures the deposition of fixed amounts of carbon on the surfaces of the catalysts, which does not affect the activity or thermal stability of the catalysts. These supported catalysts, Pt, Pd, and Ni, with cubic structures have been proven to have great potential for use in fuel processing.

Acknowledgement

The authors are thankful of NanoMite Grant (Vot. No: 5526308) for providing the funding to conduct this study. One of the authors also grateful to Basra University, Iraq for giving the financial assistance during his PhD study.

References

1 K. Sutthiumporn, T. Maneerung, Y. Kathiraser and S. Kawi, *Int. J. Hydrog. Energ.,* 2012, **37**, 11195-11207.

2 M. R. Rahimpour, Z. A. Aboosadi and A. H. Jahanmiri, *Appl. Energ*., 2011, **88**, 2691-2701.

3 W. H.Chen, B. J. Lin H. M. Lee and M. H. Huang, *Appl. Energ.* 2012, **98**, 92-101.

4 M. Sarkari, F. Fazlollahi, H. Ajamein, H. Atashi, W. C. Hecker, and L. L. Baxter, *Fuel Process Technol.,* 2014, **127**, 163-170.

5 E. R. Monazam,; R. W. Breault and R. Siriwardane, *Chem Eng. J.* 2014, **242**, 204-210.

6 A. Hasanbeigi, M. Arens and L. Price, *Renew Sustain Energ Rev.,* 2014, **33**, 645-658.

7 J. R. Rostrup-Nielsen, J. R. Anderson and M. Boudart, (Editors), *Catal. Sci. Technol.* 1984, **5**, Springer, New York.

8 E. Ruckenstein and Y. H. Hu, *Appl. Catal. A: Gen.* 1995, **133**, 149-161.

9 D. Dissanayake, M. P. Rosynek and L. H. Lunsford, *J. Phys. Chem.* 1993, **97**, 3644-3646.

10 A.T. Ashcroft, A.K. Cheetham, M. H. Green and P. F. Vernon, Nature (London), 1991, **352**, 225-231.

11 Q. Chen, J. Zhang, Q. Jin, B. Pan, W. Kong, T. Zhao and Y. Sun, *Catal. Today.,* 2013, **215**, 251-259.

12 J. Ashok and S. Kawi, *Int. J. Hydrog. Energ.,* 2013, **38**, 13938-13949.

13 Y. Liu, Z. He, L. Zhou, Z. Hou and W. Eli, *Catal. Commun.* 2013, **42**, 40-44.

14 Q. Chen, J. Zhang, Q. Jin, B. Pan, W. Kong, T. Zhaoand Y. Sun, *Catal. Today* 2013, **215**, 251-259.

15 J. Kehres, J. G. Jakobsen, J. W. Andreasen, J. B. Wagner, H. Liu, A. Molenbroekand T. Vegge, *J. Phys. Chem. C*, 2012, **116**, 21407-21415.

16 M. Garcia-Dieguez, I. S. Pieta, M. C. Herrera, M. A. Larrubia and L. J. Alemany, *Catal. Today* 2011, **172**, 136-142.

17 F. Menegazzo, M. Signoretto, P. Canton and N. Pernicone, *Appl. Catal., A*, 2012, **439**, 80-87.

18 E. Ruckenstein and Y. H. Hu, *Chem. Innov.,* 2000, **30**, 39-43.

19 M. Yu, K. Zhu, Z. Liu, H. Xiao, W. Deng and X. Zhou, *Appl. Catal. B: Environ.,* 2014. **148**, 177-190.

20 K. Tomishige, *Catal. Today*, 2004, **89**, 405-418.

21 F. W. Aldbea, N. Ibrahim, M. H. Abdullah and R. E. Shaiboub, *J. Sol-gel Sci. Technol.* 2012, **62**, 483-489.

22 P. Grange, *Catal. Rev. Sci. Eng.* 1980, **21**, 135-181.

23 H. Abimanyu, C. S. Kim, B. S. Ahn and K. S. Yoo, *Catal. Lett*., 2007, **118**, 30-35.

24 X. Chen, J. Jiang, S. Tian and K. Li, *Catal. Sci. Technol.,* 2015, **5**, 860-868.

25 M. Zhiijian, L. Ying, F. Maohong, Z. Ling, Z., *J. Chem. Eng.*, 2015, **259**, 293-302.

26 C. Hidalgo, S. Jalila, M. Alberto, M. Jose and S. Said, *J. Colloid Interface Sci.,* 2012, **382**, 67-73.

27 E. G. Mahoney, J. M. Pusel, S. M. Stagg-Williams and S. Faraji, *J.CO_2 Utiliz.,* 2014, **6**, 40-44.

28 Z. Bao, Y. Lu, J. Han, Y. Li and F. Yu, *Appl. Catal. A: Gen*., 2015, **491**, 116-126.

29 C. G. Rotaru, G. Postole, M. Florea, F. Matei-Rutkovska, V.I. Pârvulescu and P. Gelin, *Appl Catal A: Gen.,* 2015, **494**, 29-34.

30 S. Tada, T. Shimizu, H. Kameyama and T. Haneda, *Int. J. Hydro.Energ*., 2012, **37**, 5527-5531.

31 V. M. Gonzalez-Delacruz, F. Ternero, R. Peren, A. Caballero and J. P. Holgado, *Appl Catal A Gen* 2010, **384**, 1-9.

32 K. Y. Koo, H. S. Roh, Y. T. Seo, D. J. Seo, W. L. Yoon and S. B. Park, *Int. J. Hydro. Energ.,*2008, **33**, 2036-2043.

33 Z. Mei , Y. Li, M. Fan, L. Zhao and J. Zhao, *Chem. Eng. J.,* 2015, **259**, 293-302.

34 A. Djaidja, S. Libs, A. Kiennemann and A. Barama, *Catal. Today* 2006, **113**, 194-200.

35 H. W. Kim, K. M. Kang and H. Kwak, *Int. J. Hydro. Energ.,* 2009, **34**, 3351-3359.

36 L. Chen, Q. Zhu, Z. Hao, T. Zhang and Z., Xie, *Int. J. Hydro. Energ.,* 2010, **35**, 8494-8502.

37 Z. Mojović,S. Mentus and Z. Tesic, *Mater. Sci. Forum.,* 2004, **453**, 257-262.

38 A.M. Gadalla and M.E. Sommer, *Chem. Eng. Sci.*, 1989, **44**, 2825-2829.

39 A. Zecchina, G. Spoto S. Coluccia and E. Guglielminotti, *J. Chem. Soc. Faraday Trans.,* 1984, **80**, 1891-1901.

40 Y. H. Hu and E. Ruckenstein, *Acco. Chem. Res*., 2003, **36**, 791-797.

41 S. Appari, V. M. Janardhanan, R. Bauri, S. Jayanti and O. Deutschmann, *Appl. Catal. A-Gen.,* 2014, **471**, 118-125.

42 P. Djinović, G. Osojnik, B. Erjavec and A., Pintar, *Appl. Catal. B Environ.,* 2012, **125**, 259-270.

43 A. Topalidis, D. E. Petrakis and A. Ladavos, L. Loakatzikou and P. J. Pomonis, *Catal. Today.,* 2007, **127**, 238-245.

44 K. Nakagawa, M. Kikuchi, M. Nishitani-Gamo, H. Oda, H. Gamo, K. Ogawa and T. Ando, *Energ. Fuels*, 2008, **22**, 3566-3570.

45 T. Osaki and T. Mori, *J. Catal.* 2001, **204**, 89-97.

46 M. M. Barroso-Quiroga and A. E. Castro-Luna, *Inter. J. Hydro. Energ.,* 2010, **35**, 6052-6056.

47 F. Giordano, A. Trovarelli, C. Leitenburg andM. Giona, *Catal*., 2000, **193**, 273-282.

48 B. Steinhauer, M. R. Kasireddy, J. Radnik and A. Martin, *Appl. Catal., A,* 2009, **366**, 333-341.

49 S. R. Miguel, I. M. J. Vilella, S. P. Maina, D. S. Jose-Alonso, M. C. Roman-Martinez and M. J. Illan-Gomez, *Appl. Catal., A,* 2012, **435**, 10-18.

50 J. Zhu, X.Peng, L. Yao, J. Shen, D. Tong and C. Hu, *Int. J. Hydro. Energ.,* 2011, **36**, 7094-7014

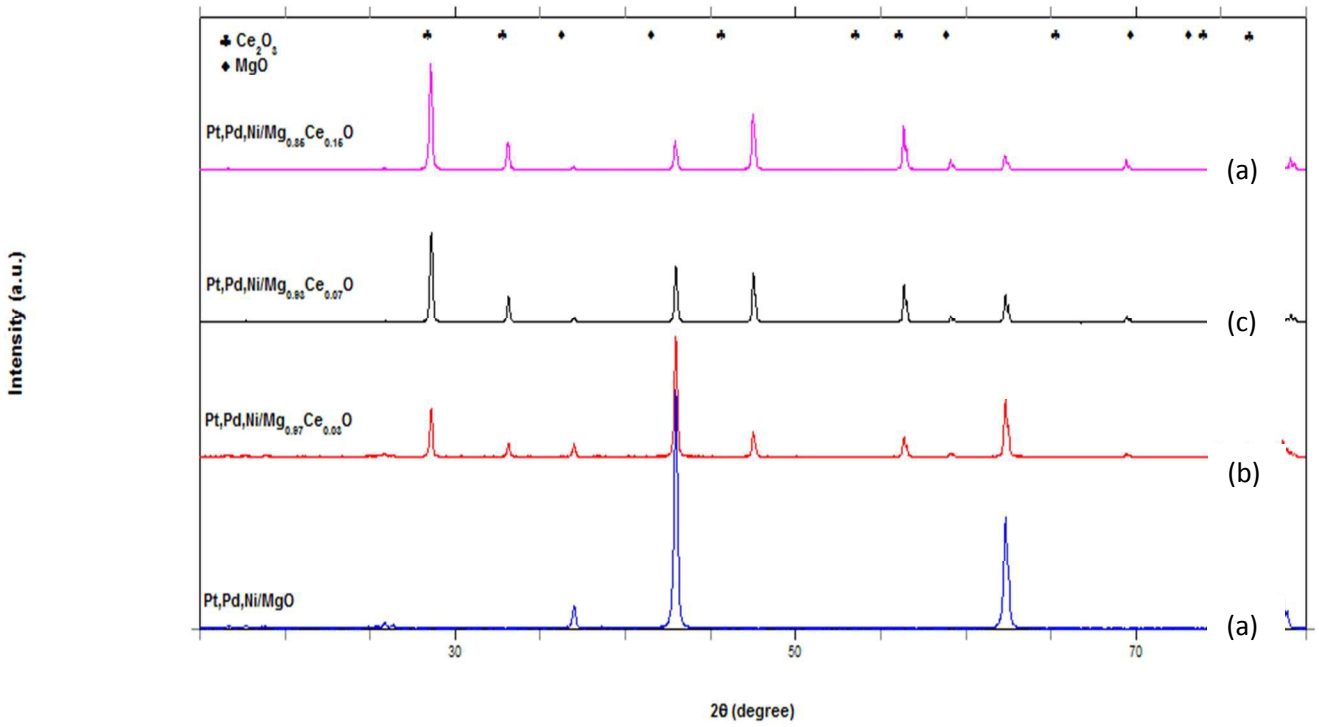

Fig. 1. XRD patterns of the catalysts (a) Pt,Pd,Ni/MgO (b) Pt,Pd,Ni/$Mg_{0.97}Ce^{3+}_{0.03}O$ (c) Pt,Pd,Ni/$Mg_{0.93}Ce^{3+}_{0.07}O$ (d) Pt,Pd,Ni/$Mg_{0.85}Ce^{3+}_{0.15}O$.

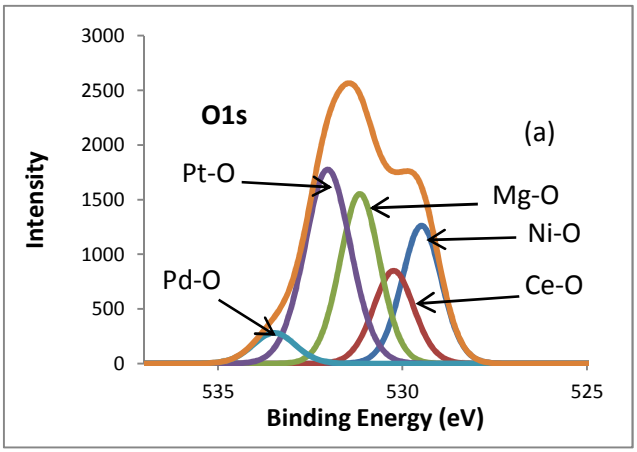

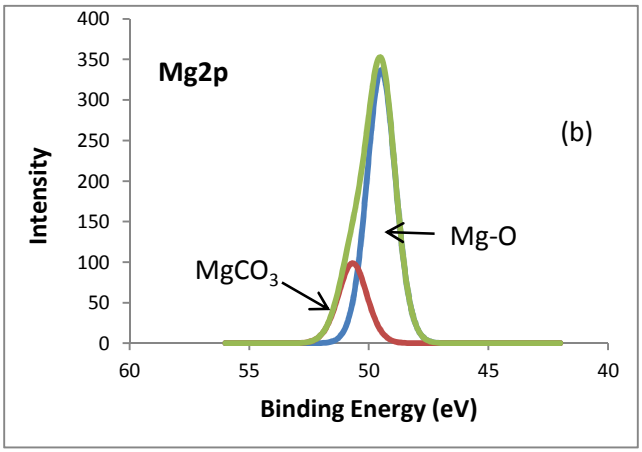

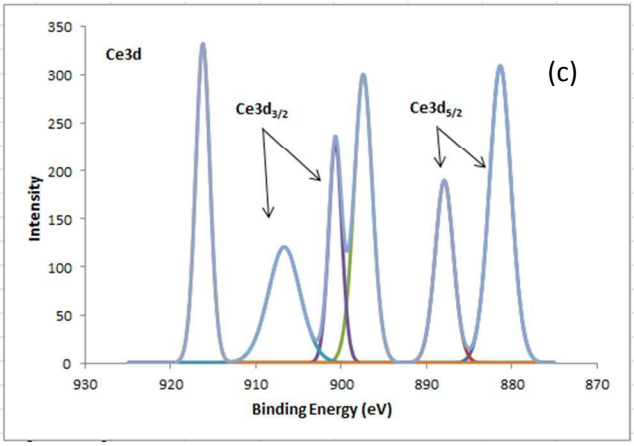

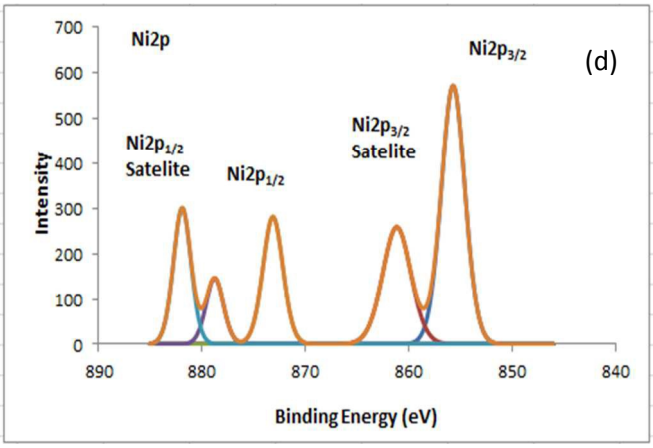

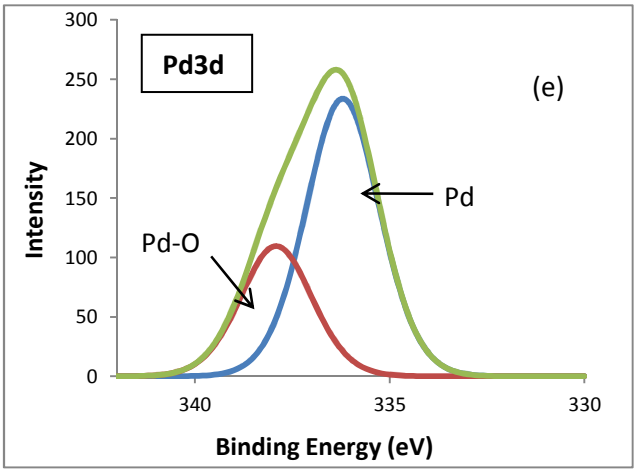

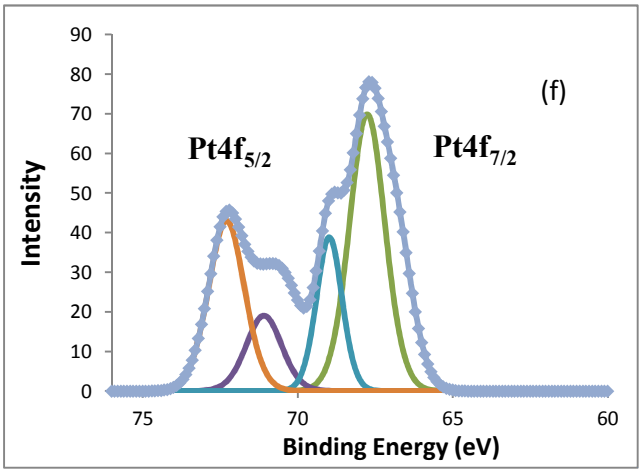

Fig. 2. XPS narrow scans of the reduced catalyst. (a) O1s b) Mg2p c) Ce3d (d) Ni2p (e) Pd3d (f) Pt4f.

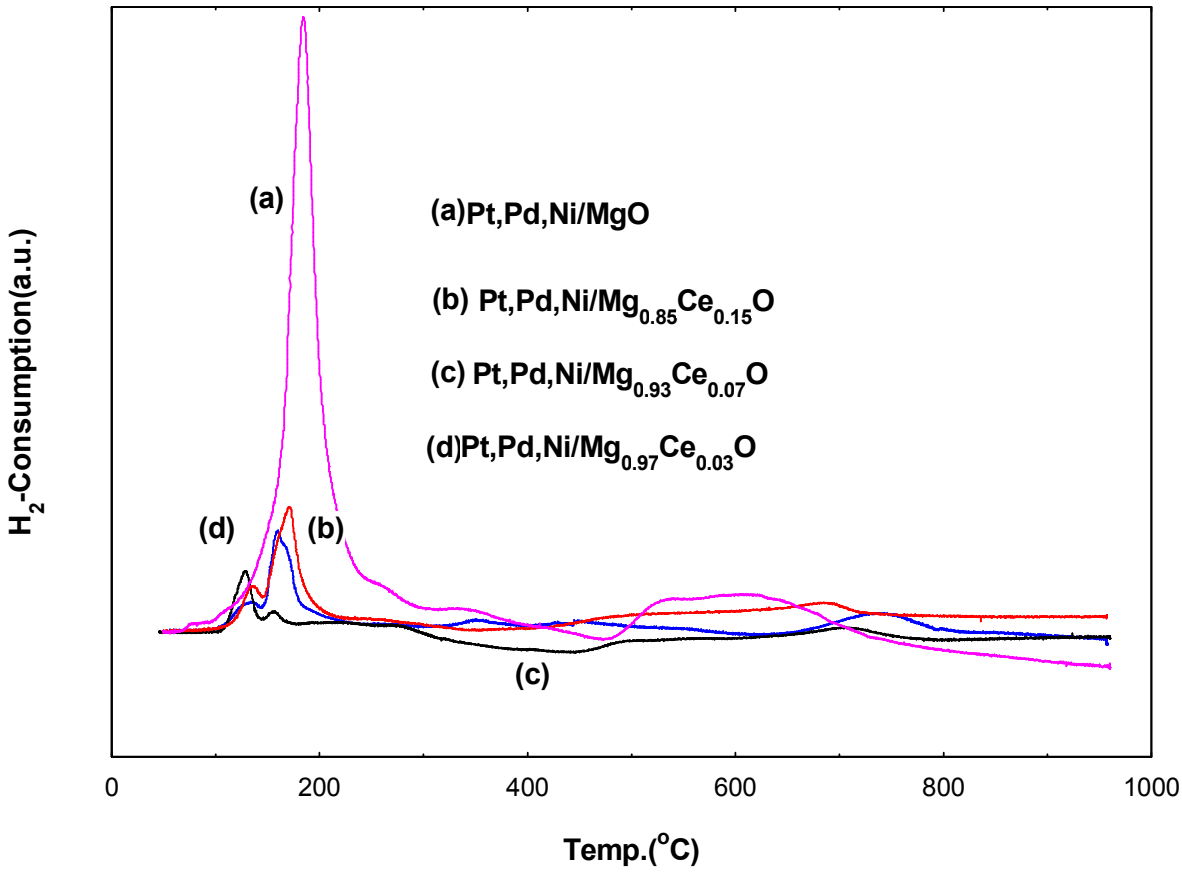

Fig. 3. TPR- H_2 profiles of catalysts reduced in a (5 % H_2/Ar) stream at a temperature ramp of 10°C/min.

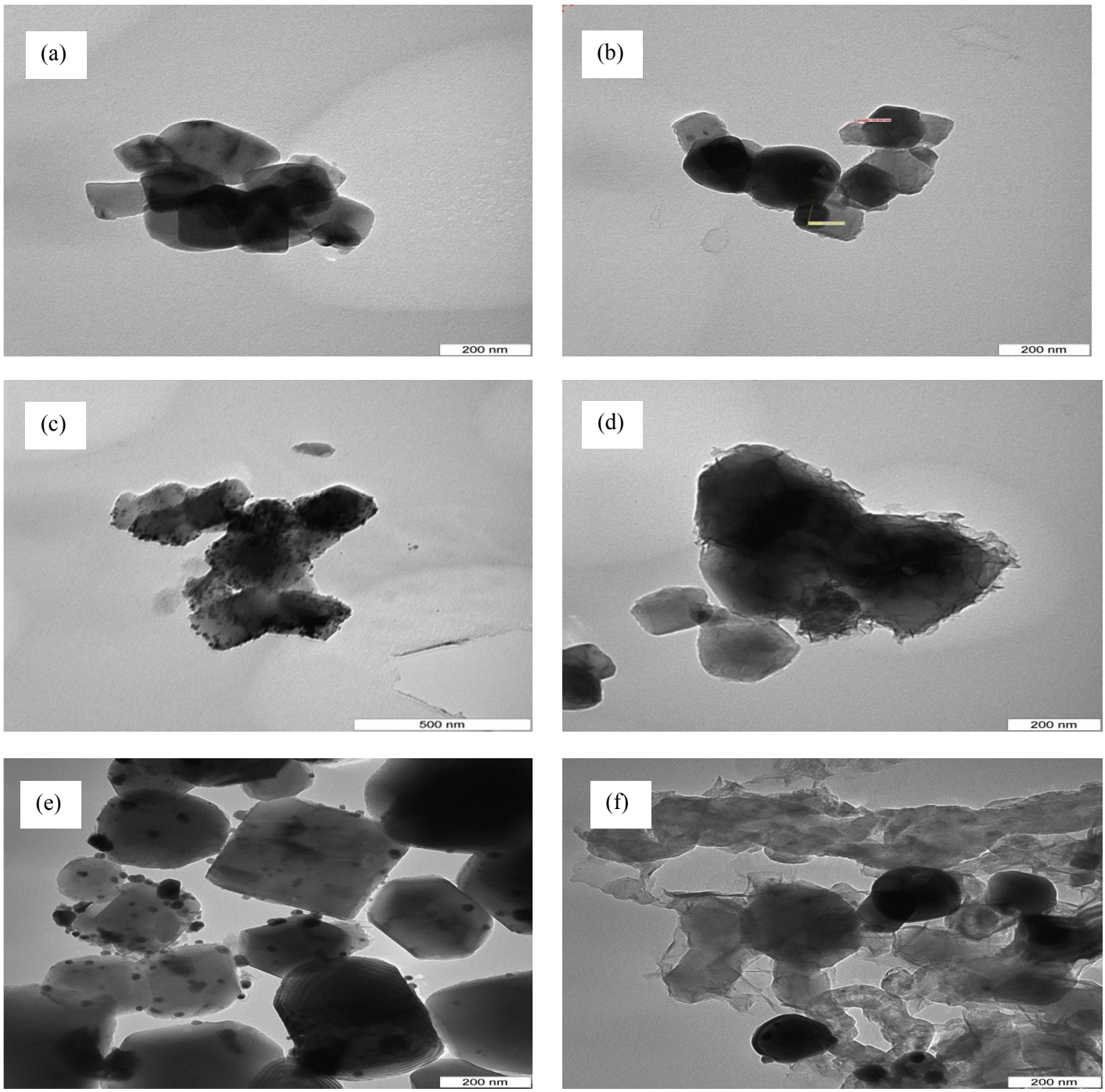

Fig. 4. TEM image of catalysts (a) Unreduced Pt,Pd,Ni/MgO (b) Unreduced Pt,Pd,Ni /$Mg_{0.97}Ce^{3+}{}_{0.03}O$ (c) Unreduced Pt,Pd,Ni /$Mg_{0.93}$ $Ce^{3+}{}_{.07}O$ (d) Unreduced Pt,Pd,Ni /$Mg_{0.85}$ $Ce^{3+}{}_{.15}O$ (e) Reduced Pt,Pd,Ni /$Mg_{0.93}$ $Ce^{3+}{}_{.07}O$ with 5% H_2 in Ar at 700°C (f) Pt,Pd,Ni/$Mg_{0.93}$ $Ce^{3+}{}_{.07}O$ after 200h reaction, at 900°C, and CH_4/CO_2 ratio 1:1.

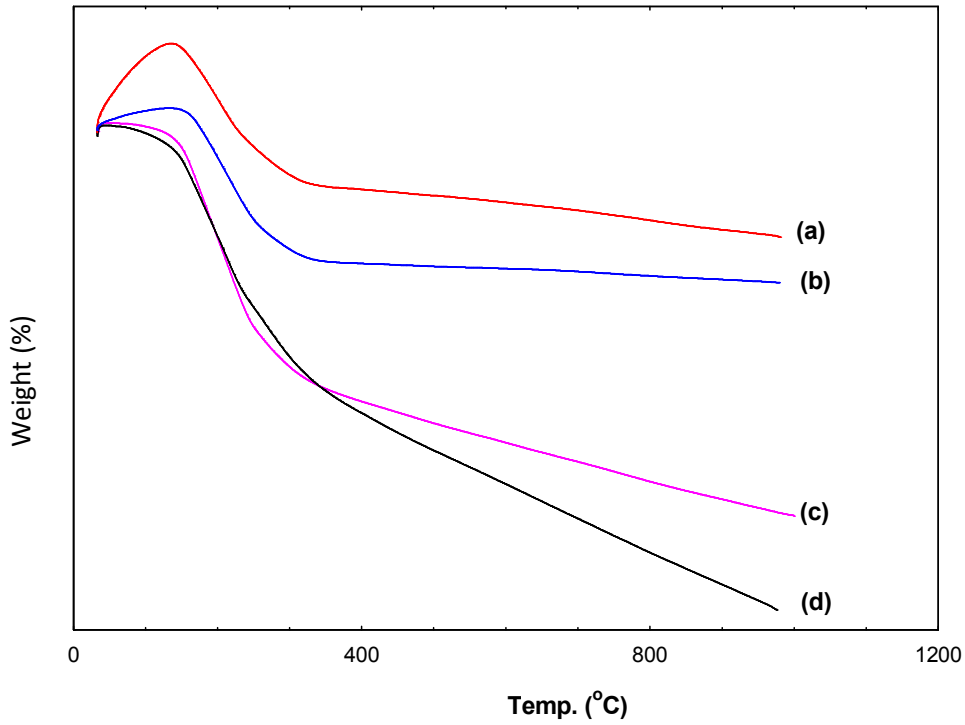

Fig. 5. TG of the catalysts (a) Pt,Pd,Ni /$Mg_{0.97}Ce^{3+}_{0.03}O$ (b) Pt,Pd,Ni/MgO (c) Pt,Pd,Ni /$Mg_{0.85}$ $Ce^{3+}_{0.15}O$ (d) Pt,Pd,Ni /$Mg_{0.93}$ $Ce^{3+}_{0.07}O$.

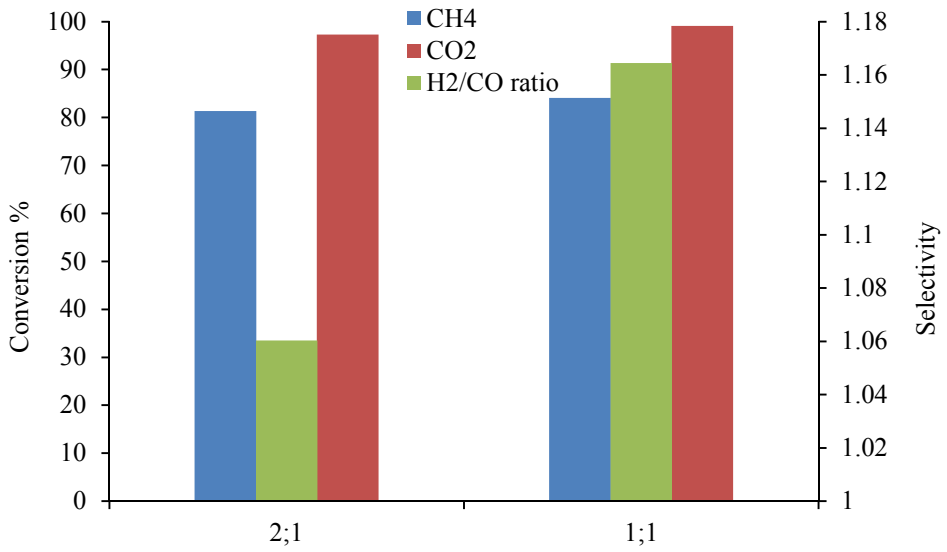

Fig. 6. The effect of changing the ratio concentration of CH_4:CO_2 reactant 1- 2:1 and 2-1:1 over the % of their conversion and H_2/CO ratio for Pt,Pd,Ni /$Mg_{0.93}Ce^{3+}_{0.07}O$ catalyst at 900°C.

37

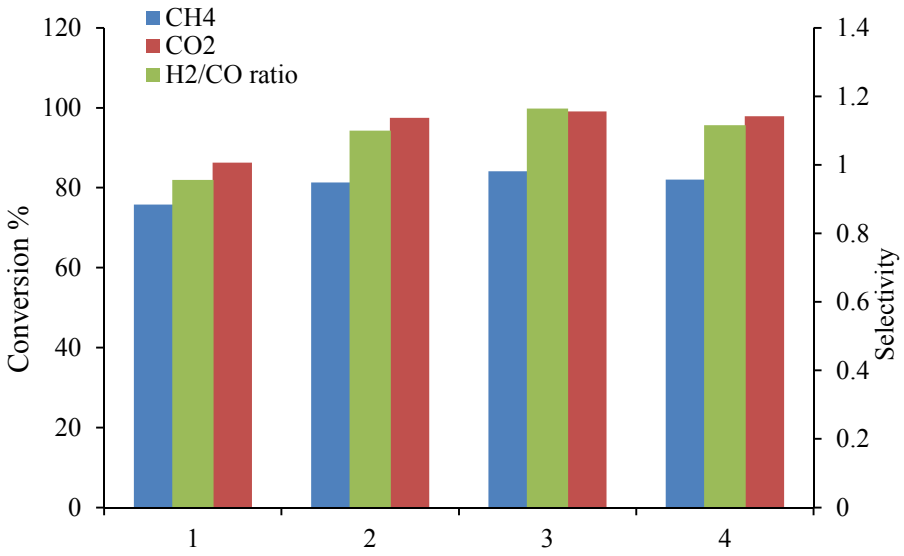

Fig. 7. The effect of using different catalysts 1) Pt,Pd,Ni/MgO, 2) Pt,Pd,Ni /$Mg_{0.97}Ce^{3+}_{0.03}O$, 3) Pt,Pd,Ni /$Mg_{0.93}Ce^{3+}_{0.07}O$, and 4) Pt,Pd,Ni /$Mg_{0.85}Ce^{3+}_{0.15}O$ on CH_4, CO_2 conversion and H_2/CO ratio at 900°C for the 1:1 ratio of CH_4:CO_2.

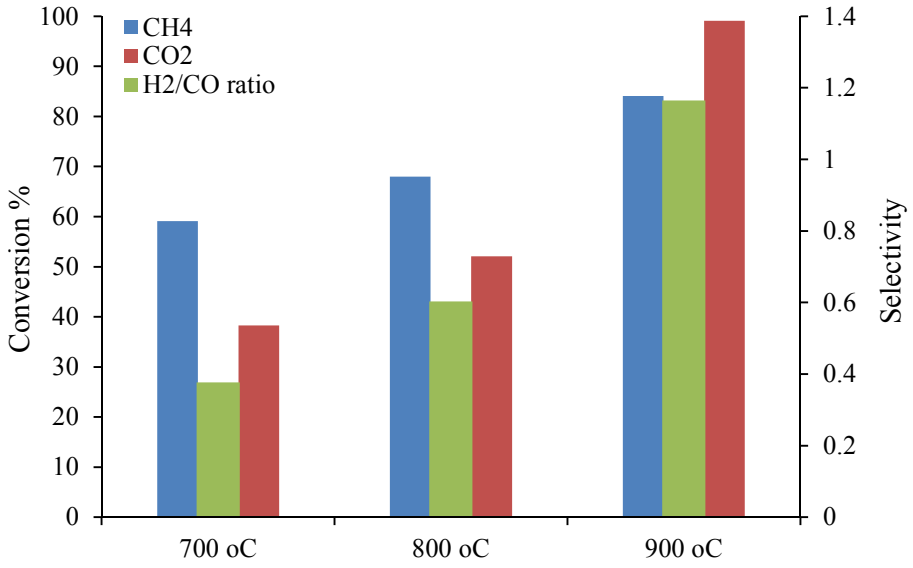

Fig. 8. The influence of temperature on the catalytic activity of the Pt,Pd,Ni/$Mg_{0.93}Ce^{3+}_{0.07}O$ catalyst. 1) 700°C 2) 800°C 3) 900°C for the 1:1 ratio of CH_4:CO_2.

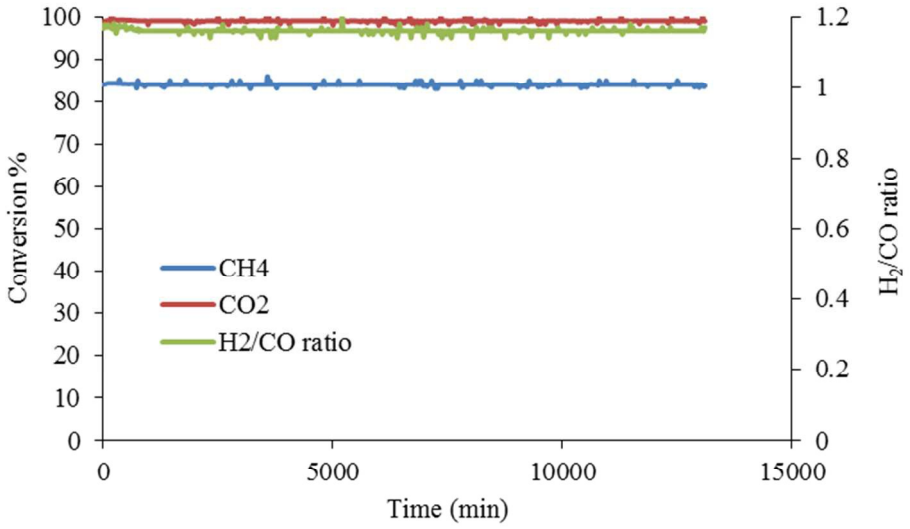

Fig. 9. Stability tests of Pt,Pd,Ni/$Mg_{0.93}Ce^{3+}_{0.07}O$ catalysts at 900°C for the 1:1 ratio of CH_4:CO_2, for 200 h. (GHSV = 15000 ml. g $cat^{-1}.h^{-1}$, atmospheric pressure).

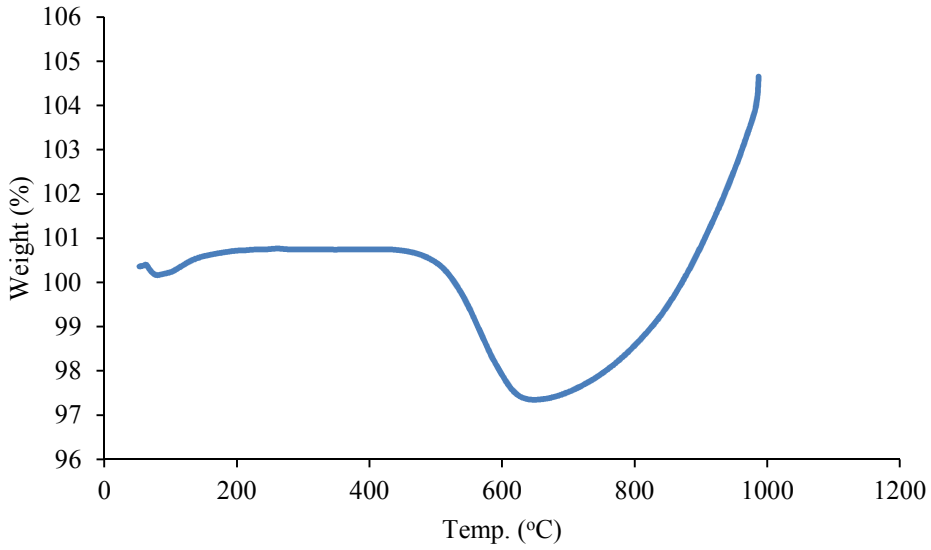

Fig. 10. TGA profiles of spent Pt,Pd,Ni/$Mg_{0.93}Ce^{3+}_{0.07}O$ catalyst (20 mL/min O_2 stream under a temperature ramp of 10°C/min).

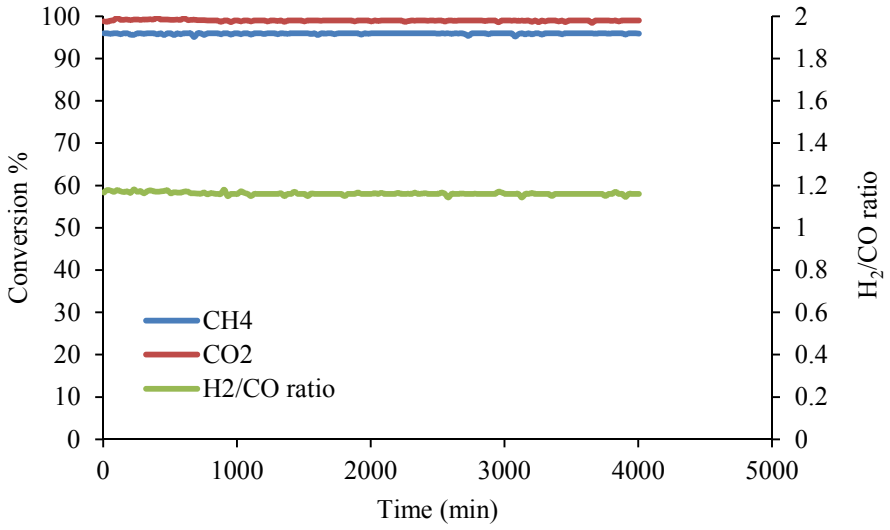

Fig. 11. DRM reaction of the Pt,Pd,Ni/$Mg_{0.93}Ce^{3+}_{0.07}O$ catalyst under 900°C with 1.25% O_2.

Table 1. Preparation of catalyst

Catalysts	Support (MgO) $Mg(NO_3)_2.6H_2O$ (g)	Promoter (Ce_2O_3) $Ce(NO_3)_3.6H_2O$ (g)	Total weight of MgO and Ce_2O_3 after calcine (g)	Impregnation of the main catalyst (1% Pt) (1% Pd) (1% Ni) (g)		
				$Pt(acac)_2$	$Pd(acac)_2$	$Ni(acac)_2$
Pt/MgO	25.0	0.0	1	0.02	0.029	0.044
$Pt,Pd,Ni/Mg_{0.97}Ce^{3+}_{0.03}O$	24.9	1.3	1	0.02	0.029	0.044
$Pt,Pd,Ni/Mg_{0.93}Ce^{3+}_{0.07}O$	23.8	3.0	1	0.02	0.029	0.044
$Pt,Pd,Ni/Mg_{0.85}Ce^{3+}_{0.15}O$	21.8	6.5	1	0.02	0.029	0.044

Table 2. Particles size measurement by XRD, TEM and XRF results

Catalysts	TEM (nm)	Crystal size (D) Debye Sherrer eq. (nm)	Ni%	Pd%	Pt%	Mg & Ce%
Pt,Pd,Ni/MgO	56	42.2	1.13	1.09	1.15	96.30
Pt,Pd,Ni/$Mg_{0.97}Ce^{3+}_{0.03}O$	68	53.3	1.18	1.11	1.19	96.17
Pt,Pd,Ni/$Mg_{0.93}Ce^{3+}_{0.07}O$	59	48.7	1.07	1.10	1.15	96.2
Pt,Pd,Ni/$Mg_{0.85}Ce^{3+}_{0.15}O$	61	48.0	1.13	1.22	1.26	96.1

Table 3. TPR-H_2 values of the different catalysts

Catalysts	Temp. ^oC	Temp. ^oC	Temp. ^oC	Temp. ^oC	Temp. ^oC	Amount H_2 gas adsorbed(μmol/g)
Pt,Pd,Ni/MgO	130	184	511	--------	--------	488.6
Pt,Pd,Ni/$Mg_{0.97}Ce^{3+}_{0.03}O$	129	169	481	502	711	429.1
Pt,Pd,Ni/$Mg_{0.93}Ce^{3+}_{0.07}O$	132	198	495	508	727	941.9
Pt,Pd,Ni/$Mg_{0.85}Ce^{3+}_{0.15}O$	135	160	490	510	735	737.7

Table 4. The main textural properties of fresh catalysts

Sample name	Specific surface area (m^2/g)	Pore volume (cm^3/g)	Pore radius (^oA)
MgO	11.1	0.21	9.9
Pt,Pd,Ni/ MgO	12.4	0.21	9.7
Pt,Pd,Ni/ $Mg_{0.97}Ce^{3+}_{0.03}O$	12.7	0.21	13.2
Pt,Pd,Ni / $Mg_{0.93}Ce^{3+}_{0.07}O$	19.8	0.22	12.5
Pt,Pd,Ni/ $Mg_{0.85}Ce^{3+}_{0.15}O$	12.9	0.21	12.4
Spent catalyst	20.2	0.23	15.6

Table 5. XRF analysis for the catalysts

Sample name	Ni%	Pd%	Pt%	Mg & Ce%
Pt,Pd,Ni / MgO	1.23	1.09	1.15	96.30
Pt,Pd,Ni / $Mg_{0.97}Ce^{3+}_{0.03}O$	1.18	1.11	1.19	96.17
Pt,Pd,Ni / $Mg_{0.93}Ce^{3+}_{0.07}O$	1.07	1.10	1.15	96.7
Pt,Pd,Ni / $Mg_{0.85}Ce^{3+}_{0.15}O$	1.13	1.22	1.26	96.1